# Supporting Information

for

## Micropollutant dynamics in Vidy Bay - A coupled hydrodynamic-photolysis model to assess the spatial extent of ecotoxicological risk

Florence Bonvin[1], Amir M. Razmi[2], David A. Barry[2] and Tamar Kohn[1]*

[1] *Environmental Chemistry Laboratory, Ecole Polytechnique Fédérale de Lausanne (EPFL), Lausanne, Switzerland*
[2] *Ecological Engineering Laboratory, Ecole Polytechnique Fédérale de Lausanne (EPFL), Lausanne, Switzerland*

*corresponding author: tamar.kohn@epfl.ch

25 pages

# List of target micropollutants and properties

Table S. 1: *Physical-chemical properties of targeted wastewater-derived compounds. MW: molecular weight; $k_H$: Henry's Law Constant*

| **Name** | **Class** | **MW** | **log Kow** | **$k_H$** | **Reference** |
|---|---|---|---|---|---|
| | | *g/mol* | | *atm $m^3$/mol* | |
| Atenolol | Beta blocker | 266.3 | 0.16 | $1.37\times10^{-18}$ | PhysProp [1] |
| Azithromycin | Antibiotic | 749.0 | 4.02 | $5.30\times10^{-29}$ | PhysProp [1] |
| Benzotriazol | Corrosion inhibitor | 119.1 | 1.44 | $1.47\times10^{-7}$ | PhysProp [1] |
| Bezafibrat | Anticholesterol | 361.8 | 4.25 | $2.12\times10^{-15}$ | PhysProp [1] |
| Carbamazepin | Antiepileptic | 236.3 | 2.45 | $1.08\times10^{-10}$ | PhysProp [1] |
| Carbendazim | Pesticide (fungicide) | 191.2 | 1.52 | $2.10\times10^{-11}$ | Toxnet [2] |
| Ciprofloxacin | Antibiotic | 331.4 | 0.28 | $5.09\times10^{-19}$ | PhysProp [1] |
| Clindamycin | Antibiotic | 425.0 | 2.16 | $2.90\times10^{-22}$ | Toxnet [2] |
| Diclofenac | Analgesic (NSAID) | 296.2 | 4.51 | $4.73\times10^{-12}$ | PhysProp [1] |
| Gabapentin | Antiepileptic | 171.2 | -1.10 | $1.81\times10^{-10}$ | PhysProp [1] |
| Gemfibrocil | Anticholesterol | 250.3 | 4.77 | $1.19\times10^{-8}$ | PhysProp [1] |
| Ketoprofen | Analgesic (NSAID) | 254.3 | 3.12 | $2.12\times10^{-11}$ | Meylan et al., 1991 [3] |
| Methylbenzotriazol | Corrosion inhibitor | 133.2 | 1.71 | $1.62\times10^{-7}$ | Lui et al., 2011 [4] |
| Metoprolol | Beta blocker | 267.4 | 1.88 | $1.40\times10^{-10}$ | PhysProp [1] |
| Metronidazol | Antibiotic | 171.2 | -0.02 | $1.69\times10^{-11}$ | PhysProp [1] |
| Norfloxacin | Antibiotic | 319.3 | -1.03 | $8.70\times10^{-19}$ | PhysProp [1] |
| Ofloxacin | Antibiotic | 361.4 | -0.39 | $4.98\times10^{-20}$ | Chemicalland21 [1 5] |
| Paracetamol | Analgesic | 151.2 | 0.46 | $6.42\times10^{-13}$ | PhysProp [1] |
| Primidon | Antiepileptic | 218.3 | 0.91 | $1.94\times10^{-10}$ | PhysProp [1] |
| Propranolol | Beta blocker | 259.3 | 3.48 | $7.98\times10^{-13}$ | PhysProp [1] |
| Simvastatin | Anticholesterol | 418.6 | 4.68 | $2.80\times10^{-10}$ | PhysProp [1] |
| Sotalol | Beta blocker | 272.4 | 0.24 | $2.49\times10^{-14}$ | PhysProp [1] |
| Sulfamethoxazol | Antibiotic | 253.3 | 0.89 | $6.42\times10^{-13}$ | PhysProp [1] |
| Trimethoprim | Antibiotic | 290.3 | 0.91 | $2.40\times10^{-14}$ | Toxnet [2] |

## Testing the biodegradability of wastewater-derived compounds

**Rationale.** For the few compounds exhibiting a slight biodegradability during activated sludge treatment, the lower bacterial density found in surface water may lead us to expect considerably slower biodegradation in the lake[6]. However, recent work showed that adaptation of oligotrophic bacterial community to low levels of biodegradable organic carbon can lead to even greater biological removal of various trace contaminants compared to the high carbon conditions typically found in wastewater treatment plants[7]. Given this possibility, laboratory incubation experiments were conducted in lake water collected above the WWTP-outfall.

**Method.** Incubation experiments were performed in lake water collected above the wastewater treatment plant outfall at a depth of 15 m (near the thermocline) in June 2013. Experiments were conducted following the OECD Guideline for the Testing of Chemicals: Aerobic Mineralisation in Surface Water – Simulation Biodegradation Test (OECD/OCDE 309). Specifically, 200 mL of lake water in sterilized Erlenmeyer flasks were spiked with low concentrations (30 and 90 $\mu$g/L) of the targeted of micropollutants. Experiments were conducted at 2 concentrations to ensure that no interactions between chemicals occurred. Initial samples were taken and flasks were placed in an incubator at 20 °C on a moving platform to ensure gentle stirring (100 rpm). Samples were taken after 2, 5 and 9 days and analyzed directly by UPLC-MS/MS, as described further in the Supporting Information.

**Results.** A summary of the removal of all 24 compounds after 2, 5 and 9 days is shown in Figure S.1, expressed as the ratio of residual concentration to the starting concentration, $C/C_0$. Considering an analytical error of ± 15%[8], no significant removal was observed after 2 days. The majority of the compounds were stable after 9 days of incubation, yet the increasing range of $C/C_0$ after 5 and 9 days indicate the biodegradation of some compounds.

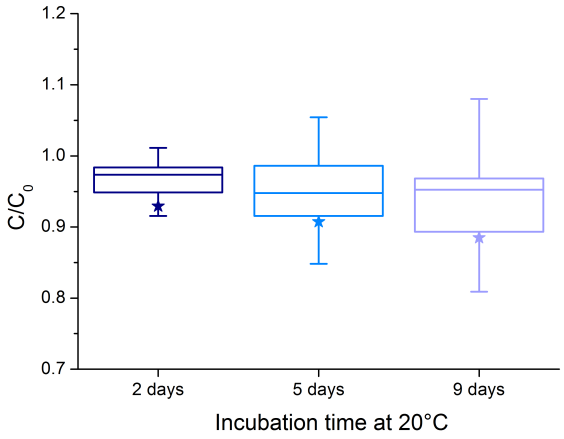


Figure S. 1: *Relative concentrations of 24 wastewater-derived micropollutants (concentration after 2, 5 and 9 days, normalized by the starting concentration: $C/C_0$). Boxes show the $25^{th}$, mean and $75^{th}$ percentiles, whiskers the 5 and $95^{th}$ percentiles, and stars the average value.*

Figure S.2 shows the relative concentrations for each individual compound after 2, 5 and 9 days. Azithromycin, bezafibrat, paracetamol and simvastatin showed a significant decrease of concentration after 5 and 9 days, indicating that they were removed biotically to some extent in lake water. The degradation of simvastatin however could not be attributed to biodegradation as it was also found to hydrolyse in milliQ water.

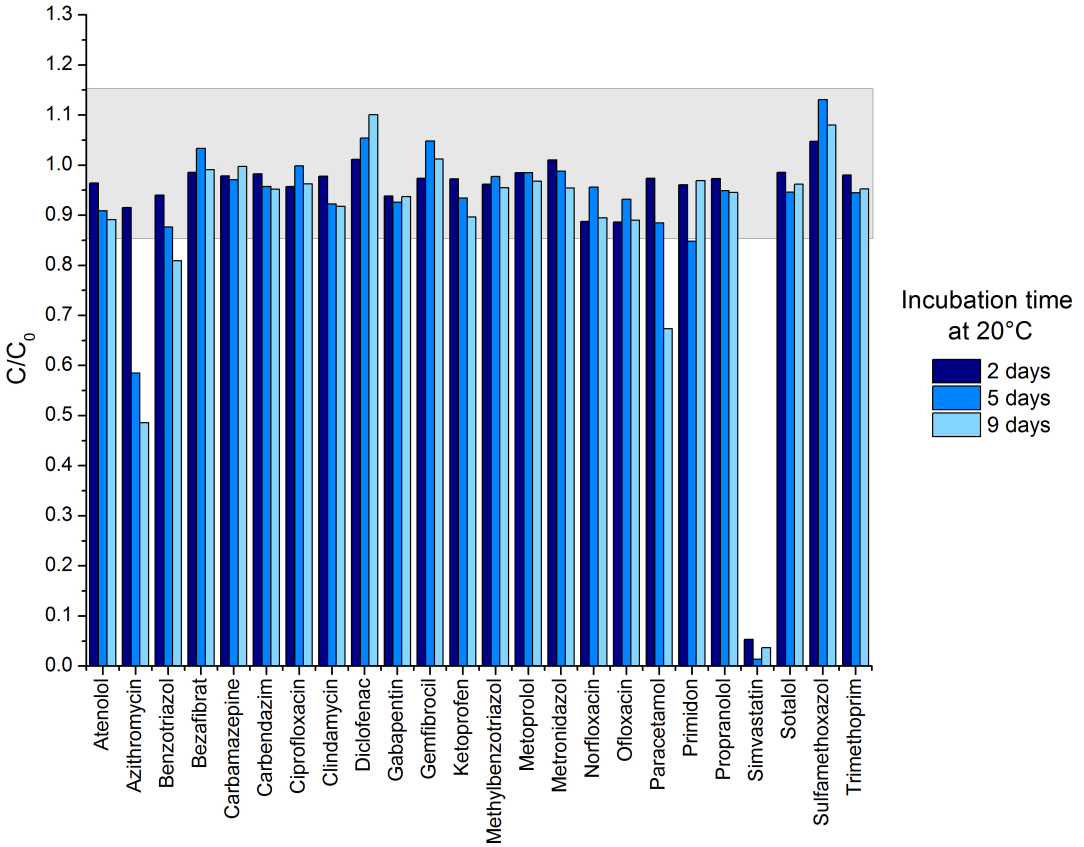


Figure S. 2: *Relative concentration of each compound incubated at 20° C in lake water after 2, 5 and 9 days. The shaded area indicates deviations from the starting concentration that are not significantly different from zero.*

## Comparison to previous work

Few studies have investigated the extent of biodegradability of pharmaceuticals within the water column of a large water body. Most studies focus on biodegradation in rivers and streams. In laboratory work, results often refer to incubation experiments containing sediments.

Biotransformation was considered the major removal mechanism in the Trinity River, an effluent dominated river. Concentrations of ethylenediamine tetraacetate, gemfibrozil, ibuprofen, metoprolol, and naproxen all decreased between 60% and 90% as the water flowed downstream. The long hydraulic retention time (2 weeks) and considerable light attenuation may explain the importance of biotransformation[9].

In contrast, work in another effluent dominated stream found no significant removal of a selection of antibiotics over 3 km after being discharged from a wastewater treatment plant. It is interesting to note that over the 3 sampling campaigns, a retention ciprofloxacin and azithromycin was observed on one occasion, yet this result was not commented [10].

Similarly, in the Roter Maine river, with an average of 18% WWTP effluent, only naproxen was eliminated during the dry period over the 13 km investigated, while bezafibrate, clofibric acid, diclofenac did not exhibit significant attenuation.The attenuation of naproxen was attributed to biotransformation [11].

Recent work in natural streams with no major WWTP input found biodegradation to be important under certain conditions: one study found photolysis to be a relevant elimination process only for diclofenac and potentially also for sotalol. For other compounds (such as bezafibrate and metoprolol), biotransformation in the sediments was also an important attenuation process along the river stretch (12-18 h residence time) [12].

The same authors report no attenuation of bezafibrate, diclofenac, metoprolol, and naproxen was observed, in another river (mean travel time 44 h). The authors hypothesized that the hydraulics and river morphology of this river were not optimal for processes in the hyporheic zone (water-sediment interface). On the other hand ibuprofen and clofibric acid were eliminated, possibly transformed by in-stream biofilms growing on submerged macrophytes. Phototransformation and sorption were ruled out as major attenuation processes [13].

These few examples illustrate the variability of results for the same compounds. Nevertheless, overall significant biodegradation was observed in rivers with longer residence times, whereas, under high flow conditions no substantial reduction can be attributed to biodegradation [11].

These results support our hypothesis that in the present setting (within the water column, 700 m from shore, no water sediment interface, no macrophytes) and given the residence times within Vidy Bay, biodegradation is not a major removal mechanism affecting the fate of micropollutants within the wastewater plume.

## Map of sampling sites and modeled area

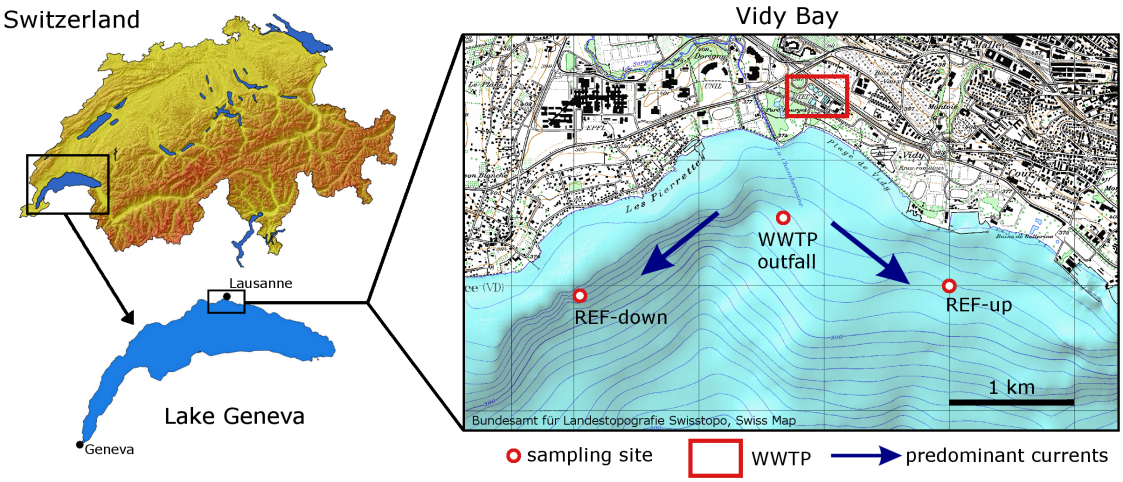


Figure S. 3: *Map of the Vidy Bay showing the sampling locations: WWTP outfall (534,672/ 151,540), REF-up (536,000/151,000) and REF down (533,048/150,920). Coordinates are in the Swiss Grid system with datum CH1903. Arrows show the two predominant current directions, which are generally parallel-to-shore*[14].

## Wind analysis for Vidy Bay

The wind scenarios chosen for the present work are based on the analysis of winds measured at the meteorological weather station in Pully (also located on the northern shore of the Vidy Bay, 2 km east of the city of Lausanne). The histogram of wind directions for a 27 year period (1981-2008) is shown in Figure S.4, for the January-March (left) and June-August (right). In both seasons, the most frequent events are winds blowing from the north (0-70°), more commonly called "Bise" and westerly winds (170-320°), called "Vent". Averaged over the entire year, available data shows that the 45% of the year winds blow from the north ("Bise"-regime) and 33% of the time they come from the west ("Vent"-regime) (Figure S.5).

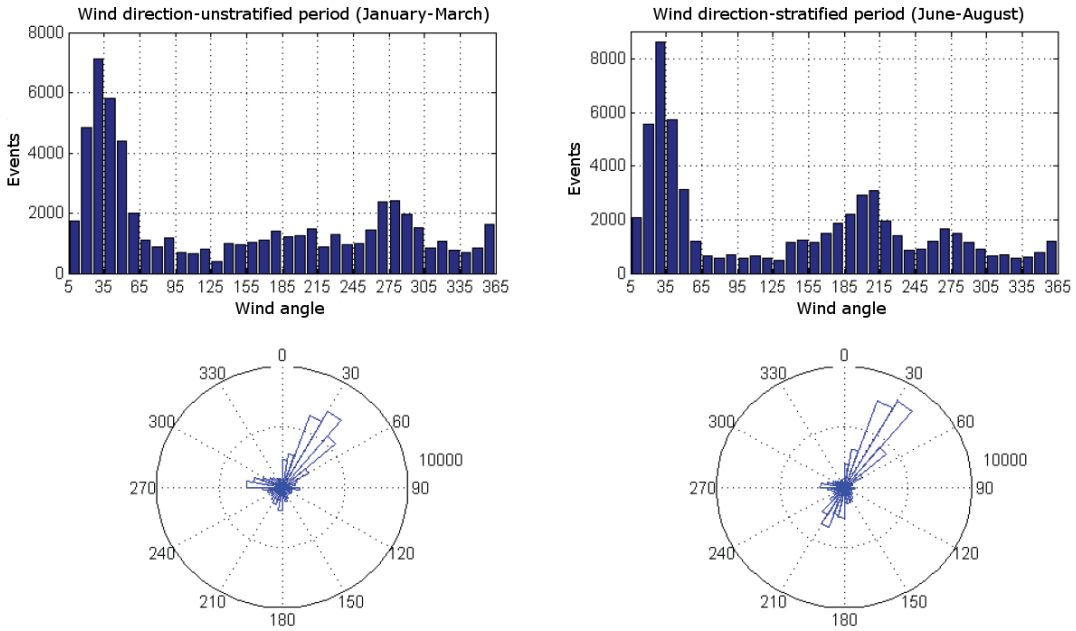


Figure S. 4: *Histogram and wind rose diagram of winds measured at Pully weather station between 1981 and 2008, for the unstratified conditions (January-March, left) and stratified conditions (June-August, right). Adapted from* [15].

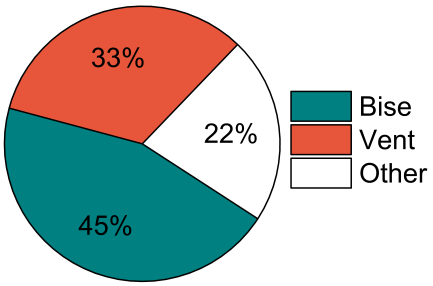


Figure S. 5: *Major wind regimes over the Vidy Bay. Bise: 0-70°; Vent: 170-320°. Compilation of wind measurements from the Pully weather station between 1981 and 2008. Adapted from* [15].

From this analysis, it is clear that Bise and Vent are the dominant wind-regimes affecting Vidy Bay. The choice of the specific wind angles (10° and 240°) for the scenarios are based on a simulation of winds above the WWTP-outfall. Specifically, meteorological data measured at various weather stations along the lake are the input of an atmospheric prediction model (COSMO-2 [16]), yielding simulated wind directions over the entire lake. The results of the simulations above the WWTP-outfall are shown in Figure S.6. The dominant wind angles are 10° and 240°, which were thus chosen as representative of the "Bise" and "Vent"-regime, respectively.

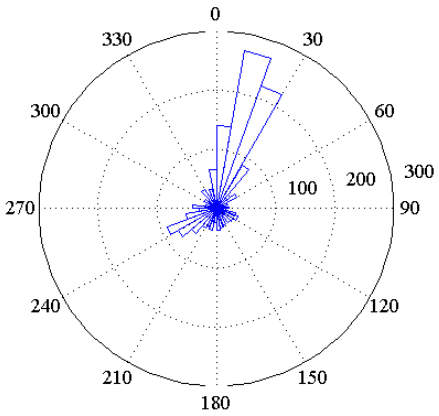


Figure S. 6: *COSMO-2 simulation of wind directions above WWTP outfall.*

# Details on direct photolysis experiments and analytical method

## Detailed method for direct photolysis experiments

Solutions of a mixture of up to nine micropollutants, with individual concentrations ranging between 15 and 80 $\mu$g $L^{-1}$ in 1 mM bicarbonate-buffered Nanopure water (pH 8.4) were irradiated between 2 and 76 h by a Sun 2000 Solar Simulator (ABET Technologies, Milford, Connecticut) equipped with a 1000 W Xe lamp and an AM1.5 filter. The starting concentration of each compound corresponded to 10-times its limit of detection (LOD). As such, we monitored a 90% decay, while minimizing light screening by the target compounds. The compounds were grouped into mixtures based on their susceptibility to direct photolysis determined in preliminary experiments.

The irradiance of the solar simulator was determined spectroradiometrically (Model ILT-900-R, International Light) before and after each experiment. The absolute irradiance was calibrated using chemical actinometry (p-nitroanisole (pNA)) and was 76 W $m^{-2}$ between 280 and 430 nm and showed no day-to-day variation (lamp spectrum shown in Figure S.7). The irradiated solutions (400 mL) in amber glass beakers were continuously stirred , and their temperature was maintained at ca. 19°C using a water-filled tray, connected to a recirculation cooler (F240 Recirculating Cooler, Julabo). Identical solutions were left in the dark during each experiment to serve as dark controls. Moreover, mixtures containing double the starting concentration of each compound (between 30 and 160 $\mu$g $L^{-1}$) were photolyzed concurrently, to determine if second-order reactions between compounds in the mixture were contributing to the observed degradation. At selected time points (minimum 7), 1.2 mL samples were collected to monitor the parent compound concentration decrease over time. The samples were transferred to amber glass vials, were maintained at 4°C after collection and were analyzed within 48 h by ultra-performance liquid chromatography (Acquity UPLC system, Waters) coupled to a tandem mass spectrometer (MS/MS, XEVO, Waters). The experiments were repeated three times. Data acquisition and processing was performed using Masslynx. In parallel, absorbance spectra for all solutions were collected with a UV-vis 2550 Spectrophotometer (Shimadzu Scientific Instruments) at various irradiation time points to assess the change in absorbance over time and wavelength. Time-averaged values were used to correct for light screening.

**Absolute and normalized spectrum of the solar simulator and simulated solar spectrum**

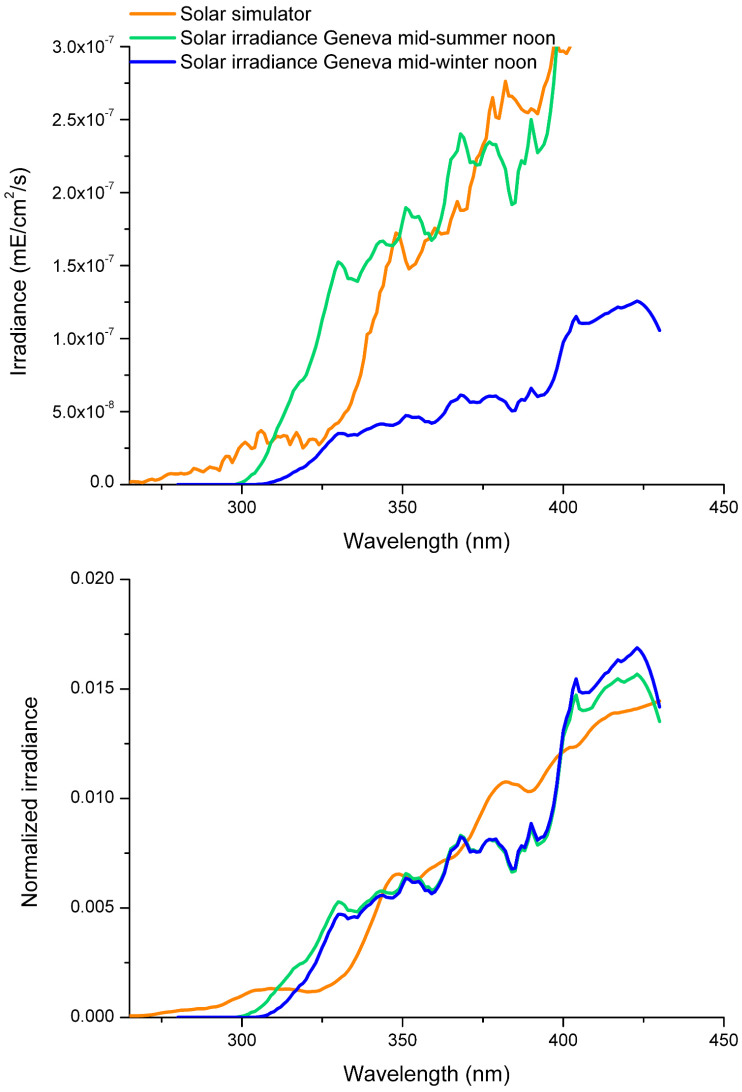


Figure S. 7: *Top: Absolute irradiance of the solar simulator and of the computed SMARTS solar irradiance for a sunny day at 47° N for a summer scenario ($21^{st}$ June) and winter scenario ($21^{st}$ December). Bottom: Normalized irradiance of the solar simulator and of the computed SMARTS solar irradiance for a sunny day at 47° N (Geneva) for a summer scenario ($21^{st}$ June) and winter scenario ($21^{st}$ December) Values are normalized over the wavelength interval of 265–430 nm. Note that, though the solar simulator spectrum extends below 280 nm, excess UVB compared to the solar spectrum only amounts to 1% of the total intensity.*

**Monitoring concentration decay in photodegradation experiments via UPLC-MS/MS**

Compound decay was monitored via ultra-performance liquid chromatography (Acquity UPLC system, Waters) coupled to a tandem mass spectrometer (MS/MS, XEVO, Waters).

1) Ultra-performance liquid chromatography

**Mobile phases:** Two distinct mobile phases were used for correct separartion and detection of all target micropollutants:
Eluent A-basic: 94.8% $H_2O$ + 5% ACN + 0.2% $NH_4OH$
Eluent B-basic: 5% $H_2O$ + 94.8% ACN + 0.2% $NH_4OH$
Eluent A-neutral: 95% $H_2O$ + 5% ACN
Eluent B-neutral: 5% $H_2O$ + 95% ACN
**Column:** Acquity UPLC BEH C18 1.7 um, 2.1 x 50 mm
**Chromatographic conditions:** 0.4 mL/min, 17 min run time, column temperature: 30°C
**Gradient:** 0–2.5 min: 95% A; 2.5–3 min ramp to 80% A; 3–11 min: ramp down to 5% A; 11–13.5 min: stabilize at 5% A; 13.5–14 min: ramp up to 95% A; 14–17 min: equilibrate at 95% A.

2) Mass spectrometry

See Table S.2 below.

Table S. 2: *Analytical method for MS/MS analysis of targeted wastewater-derived micropollutants. Parent mass, daughter fragment mass, cone voltage (CV), collision energy (CE), UPLC method (basic or neutral mobile phase) and retention time (RT) of compound. *TQD: compounds analyzed on a different mass spectrometer (TQD, Waters) with a previously described method*[17].

| **Compound** | **Parent mass** | **Daughter mass** | **CV (V)** | **CE (eV)** | **UPLC method** | **RT (min)** |
|---|---|---|---|---|---|---|
| atenolol | 267.37 | 74.04 | 32 | 22 | basic | 3.60 |
| | | 145.11 | 32 | 24 | | |
| azithromycin | 749.88 | 83.08 | 53 | 56 | basic | 8.90 |
| | | 116.10 | 53 | 46 | | |
| benzotriazol | | | *TQD | | | |
| bezafibrate | 360.10 | 154.00 | 20 | 30 | basic | 3.64 |
| | | 274.00 | 20 | 15 | | |
| carbamazepine | 237.30 | 165.15 | 33 | 36 | basic | 4.90 |
| | | 179.07 | 33 | 35 | | |
| carbendazim | 192.10 | 132.10 | 24 | 28 | neutral | 3.70 |
| | | 160.10 | 24 | 18 | | |
| ciprofloxacin | 332.10 | 231.10 | 30 | 40 | basic | 0.53 |
| | | 288.10 | 30 | 18 | | |
| clindamycin | 425.44 | 126.18 | 38 | 26 | basic | 6.34 |
| | | 377.33 | 38 | 20 | | |
| diclofenac | | | *TQD | | | |
| gabapentine | 172.27 | 119.11 | 25 | 22 | neutral | 3.80 |
| | | 137.13 | 25 | 15 | | |
| gemfibrozil | 249.00 | 121.00 | 20 | 15 | basic | 4.00 |
| | | 127.00 | 20 | 10 | | |
| ketoprofen | 255.07 | 104.89 | 22 | 22 | neutral | 1.29 |
| methylbenzotriazol | | | *TQD | | | |
| metoprolol | | | *TQD | | | |
| metronidazole | 172.00 | 82.00 | 21 | 21 | neutral | 1.04 |
| | | 128.00 | 22 | 15 | | |
| norfloxacin | 320.10 | 233.00 | 30 | 25 | basic | 0.52 |
| | | 276.10 | 30 | 18 | | |
| ofloxacin | 362.10 | 261.10 | 30 | 26 | basic | 0.88 |
| | | 318.10 | 30 | 20 | | |
| paracetamol | 152.00 | 93.00 | 20 | 25 | neutral | 0.83 |
| | | 110.00 | 20 | 15 | | |
| primidon | 219.28 | 91.08 | 20 | 20 | neutral | 3.42 |
| | | 162.16 | 20 | 11 | | |
| propranolol | 260.10 | 116.00 | 25 | 18 | basic | 7.42 |
| | | 183.10 | 25 | 18 | | |
| simvastatin | 419.54 | 199.25 | 24 | 17 | neutral | 8.75 |
| | | 285.31 | 24 | 12 | | |
| sotalol | 273.33 | 133.20 | 20 | 26 | basic | 0.58 |
| | | 213.16 | 20 | 18 | | |
| sulfamethoxazol | 254.00 | 92.00 | 27 | 26 | neutral | 1.23 |
| | | 156.00 | 27 | 16 | | |
| trimetoprim | 291.00 | 123.00 | 39 | 27 | basic | 3.76 |
| | | 230.00 | 39 | 24 | | |

## Detailed photolysis calculations

### Light screening corrections and calibration of light source

The degradation of all compounds followed first order kinetics and degradation rate constants for each compound $i$ ($k_{direct,i}$ ) were calculated using the slope of $\ln(A_t/A_0)$ plotted against time, where $A_t$ refers to the peak area of chromatograms at time $t$, and $A_0$, the initial peak area. A light-screening factor was used to account for the fact that in some solutions the average light intensity in the beaker was lower than in optically dilute solutions. The screening factor depends on the absorbance of solution, $\alpha(\lambda)$, and on the depth of the well-mixed solution, $z$, according to equation S1.

$$\mathrm{SF}(\lambda) = \frac{1-10^{-\alpha(\lambda)\,z}}{2.303\,\alpha(\lambda)\,z} \tag{S1}$$

The observed direct photolysis degradation rate constant, $k_{direct,i}$ , can then be corrected to yield a photolysis rate constant representative of an optically dilute system:

$$k^0_{direct,i} = \frac{k_{direct,i}}{\mathrm{SF}(\lambda)} \tag{S2}$$

All reported values are corrected for light screening.

The direct photolysis quantum yields ($\Phi_i$) for each compound ($i$) were then calculated as follows:

$$\Phi_i = \frac{k^0_{direct,i}}{k^0_{abs,i}} \tag{S3}$$

The specific rate of light absorbtion, $k^0_{abs,i}$, in an optically dilute solution is a function of the light intensity, $I_\lambda$, and the decadic molar extinction coefficient of the compound, $\varepsilon_\lambda$:

$$k^0_{abs,i} = 2.303 \sum_\lambda I_\lambda\,\varepsilon_\lambda \tag{S4}$$

The light intensity, $I_\lambda$ , of the solar simulator was calibrated using a chemical actinometer, p-nitroanisole (pNA). To do so, the light intensity measured spectroradiometrically, $I_m(\lambda)$, was normalized by the total measured intensity over the relevant wavelength interval to give the normalized light intensity, $\rho_\lambda$ :

$$\rho_\lambda = \frac{I_m(\lambda)}{\sum_\lambda^{280-430\mathrm{nm}} I_m(\lambda)} \tag{S5}$$

The actual total light intensity, $I_{act}$, was determined using a pNA actinometry

$$I_{act} = \frac{k_a c t}{2.303\,\Phi_{act}\sum_\lambda(\varepsilon_{\lambda,act}\times\rho_\lambda)} \tag{S6}$$

where $k_{act}$ is the first-order degradation rate constant of pNA photolysis, $\Phi_{act}$ the known quantum yield of pNA[18] and $\varepsilon_{act}(\lambda)$, the decadic molar extinction coefficient of the actinometer. The absolute intensity at a given wavelength is then:

$$I_\lambda = I_{act}\,\rho_\lambda \tag{S7}$$

**Error calculations**

The direct photolysis rate constants correspond to average values of 2–3 experiments, each with its respective error (95% confidence interval). Accordingly, the errors associated to the average direct photolysis rate constant correspond to the propagated errors of single experiments. The uncertainty associated with calculated values, such as the specific rate of light absorption or the quantum yield, was also calculated using basic propagation of uncertainty rules and certain assumptions regarding the errors of certain quantities. More explicitly we assume a 10% error on the irradiance measurements as for the molar absorptivity of each compound. We also assume that the errors are independent of wavelength.

**Light screening factor in lake water ($\mathrm{SF}_{lake}(z)$):**

The near-surface specific rate of light absorption for a given substance $i$, can be calculated as follows over the relevant wavelength absorption range:

$$k^0_{abs,sun,i} = 2.303 \sum_{280\mathrm{nm}}^{\lambda_{\mathrm{range}}} \varepsilon_i(\lambda)\, \mathrm{I}_{sun}(\lambda) \tag{S8}$$

$\varepsilon_i$ denotes the decadic molar extinction coefficient for substance $i$ and was determined at pH 8.3 using a UV-vis 2550 Spectrophotometer (Shimadzu Scientific Instruments). $\mathrm{I}_{sun}(\lambda)$ represents the computed solar irradiance for the chosen scenario (summer or winter).
The lake water screening factor for a given depth $z$ is the ratio of the specific rate of light absorption at that depth, $k^z_{abs,sun,i}$, and the near-surface specific rate of light absorption, $k^0_{abs,sun,i}$:

$$\mathrm{SF}_{lake}(z) = \frac{k^z_{abs,sun,i}}{k^0_{abs,sun,i}} = \frac{\mathrm{I}_{sun}(\lambda)\, \varepsilon_i\, (1-10^{-z\, \alpha_D(\lambda)})}{\mathrm{I}_{sun}(\lambda)\, \varepsilon_i\, 2.303\, z\, \alpha_D(\lambda)} = \frac{1-10^{-z\, \alpha_D(\lambda)}}{2.303\, z\, \alpha_D(\lambda)} \tag{S9}$$

where $\alpha_D(\lambda)$ denotes the diffuse attenuation coefficient of lake water. It can be approximated by[19]:

$$\alpha_D(\lambda) = 1.2\, \alpha_{lake}(\lambda) \tag{S10}$$

Though wavelength-dependent, it can be approximated by using the value from a single wavelength where $k_{abs}$ is maximal, which in the case of nitrate and most of the targeted compounds is near 320 nm. For Lake Geneva water, an average lake water absorbance at 320 nm, $\alpha_{lake}$(320 nm), of 0.02 $\mathrm{cm}^{-1}$ was measured. The absorbance values did not vary significantly over the entire sampling period.

**Calculation of bimolecular reaction rate constant with hydroxyl radical**

Equation 2 from text:

$$k^0_{tot,i} - k^0_{direct,i} = k'_{{}^{\bullet}OH,i} = [{}^{\bullet}OH]_{ss}\, k_{{}^{\bullet}OH,i}$$

Values from literature (Table S4 below) were used to estimate the $[{}^{\bullet}\mathrm{OH}]_{ss}$ in each experimental beaker containing a mixture of substances with known (from literature) and unknown bimolecular rate constants with ${}^{\bullet}\mathrm{OH}$, via equation 2. Consequently, unknown bimolecular rate constants were calculated with the estimated $[{}^{\bullet}\mathrm{OH}]_{ss}$ from the corresponding experimental beaker.

**Estimation of $[^{\bullet}OH]_{ss,lake}$**

The steady state concentration of hydroxyl radicals in Lake Geneva, $[^{\bullet}OH]_{ss,lake}$, was calculated based on average measured levels of nitrate (0.029 mM) and scavenging species, such as $HCO_3^-$, $CO_3^{2-}$ and dissolved organic carbon content (see below). The estimation of the steady state concentration of hydroxyl radicals extrapolated to 24 h on a sunny day yields maximal values of $1.7\times10^{-17}$ and $3\times10^{-18}$ M for the summer and winter scenarios respectively. The SF in equation 4 accounts for the reduction in hydroxyl radical production with depth, as less light becomes available for the photolysis of nitrate.

The concentration of hydroxyl radicals in surface waters can be approximated by the ratio of the rates of production and consumption of $^{\bullet}OH$[19]:

$$[^{\bullet}OH] = \frac{k_{abs,NO_3^-}\,\Phi_{f,NO_3^-}\,[NO_3^-] + k_{abs,NO_2^-}\,\Phi_{f,NO_2^-}\,[NO_2^-]}{k'_{^{\bullet}OH,DOC}\,[DOC] + k'_{^{\bullet}OH,HCO_3^-}\,[HCO_3^-] + k'_{^{\bullet}OH,CO_3^{2-}}\,[CO_3^{2-}]} \quad \text{(S11)}$$

The values used in equation S11 are given in Table S.3.

Table S. 3: *Parameters used in equation S11*

| | **Summer** | **Winter** | **Unit** | |
|---|---|---|---|---|
| $k_{abs,NO_3^-}$ | $1.31\times10^{-5}$ | $1.89\times10^{-6}$ | $M^{-1}\,s^{-1}$ | specific rate of light absorption of nitrate, noon |
| $\Phi_{f,NO_3^-}$ | 0.007 | 0.007 | - | quantum yield of $^{\bullet}OH$ formation by nitrate |
| $[NO_3^-]$ | $2.9\times10^{-5}$ | $2.9\times10^{-5}$ | M | nitrate concentration (measured) |
| $[NO_2^-]$ | 0 | 0 | M | nitrite concentration (measured) |
| $k'_{^{\bullet}OH,DOC}$ | $2.5\times10^{4}$ | $2.5\times10^{4}$ | $(mg\,C)^{-1}s^{-1}$ | reaction rate constant between $^{\bullet}OH$ and DOC[20] |
| [DOC] | 1.4 | 1.1 | $mg\,C\,L^{-1}$ | dissolved organic carbon concentration (measured[21]) |
| $k'_{^{\bullet}OH,HCO_3^-}$ | $1\times10^{7}$ | $1\times10^{7}$ | $M^{-1}\,s^{-1}$ | reaction rate constant between $^{\bullet}OH$ and $HCO_3^-$[22] |
| $[HCO_3^-]$ | $2.25\times10^{-3}$ | $2.25\times10^{-3}$ | M | bicarbonate concentration (calculated) (a) |
| $k'_{^{\bullet}OH,CO_3^{2-}}$ | $4\times10^{8}$ | $4\times10^{8}$ | $s^{-1}$ | reaction rate constant between $^{\bullet}OH$ and $CO_3^{2-}$[22] |
| $[CO_3^{2-}]$ | $3.73\times10^{-5}$ | $9.8\times10^{-6}$ | $M^{-1}\,s^{-1}$ | carbonate concentration (b) |
| $[OH]_{ss,noon}$ | $3.95\times10^{-17}$ | $6.79\times10^{-18}$ | M | $^{\bullet}OH$ steady state concentration, noon |
| $[OH]_{ss,24h}$ | $1.74\times10^{-17}$ | $3\times10^{-18}$ | M | $^{\bullet}OH$ steady state concentration, 24h |

(a) $[HCO_3^-] = 2\,[Ca^{2+}]$

(b) $\log[CO_3^{2-}] = pH - pK_a + \log[HCO_3^-]$

**Results from photodegradation experiments**

see Table S.4 below

Table S. 4: *Direct and indirect photolysis parameters determined for the 24 target micropollutants: $k^0_{direct,i}$: direct photolysis rate constant measured in buffered solution under the solar simulator, and resulting quantum yield (QY). These values are not applicable (n.a.) to compounds which do not absorb light beyond 280 nm. $k_{\cdot OH,i}$: bimolecular rate constant between compound and hydroxyl radical; $\tau_{summer}$ and $\tau_{winter}$: predicted environmental half-life based on $k^{24h}_{env,tot,i}(z)$ (equation 5 in text, z = 50 cm); percent indirect: contribution of indirect to total photolysis; PNEC: predicted no-effect concentration.*

| **Compound Name** | $k^0_{direct,i}$ ($h^{-1}$) | $\Phi$ | $\Phi$-**literature** | $k_{\cdot OH,i}$ ($M^{-1}$ $s^{-1}$) | **Reference for** $k_{\cdot OH,i}$ | $\tau_{summer}$ (h) | $\tau_{winter}$ (h) | **Percent indirect** | **PNEC** ($ngL^{-1}$) |
|---|---|---|---|---|---|---|---|---|---|
| atenolol | 0.018 ± 0.002 | 0.019 ± 0.004 | | 7.5 ± 0.3 | Ji et al.[23] | 2916 | 20525 | 87% | 33400 |
| azithromycin | n.a. | n.a. | | 2.9 | Dodd et al.[24] | 9539 | 55327 | 100% | 10 |
| benzotriazol | 0.11 ± 0.01 | 0.015 ± 0.004 | 0.009 ± 0.0002[25] | 14 ± 2 | Vel Leitner et al.[26] | 1474 | 10861 | 86% | 30000 |
| bezafibrat | 0.061 ± 0.004 | 0.055 ± 0.011 | | 7.4 ± 1.2 | Huber et al.[27] | 3737 | 21682 | 100% | 1191 |
| carbamazepin | 0.006 ± 0.001 | 0.00015 ± 0.00004 | 0.0003 ± 0.0004[25,28] | 5.0 ± 0.6 | Wols et al.[28] | 1293 | 9860 | 27% | 2500 |
| carbendazim | 0.009 ± 0.001 | 0.00051 ± 0.00012 | 0.002[28] | 5.9 ± 0.1 | Wols et al.[28] | 4319 | 27237 | 95% | 100 |
| ciprofloxacin | 10 ± 1 | 0.037 ± 0.009 | 0.012 ± 0.002[28] | 5.94 ± 1.72 | Wols et al.[28] | 0.26 | 1.2 | 0% | 5 |
| clindamycin | n.a. | n.a. | | 22 ± 21 | *this study* | 1254 | 7275 | 100% | 1000000 |
| diclofenac | 28 ± 3 | 0.76 ± 0.19 | 0.17 ± 0.18[25,28] | 8.4 ± 0.8 | Wols et al.[28] | 0.41 | 2.1 | 0.01% | 100 |
| gabapentin | n.a. | n.a. | | 1.4 ± 0.4 | *this study* | 19497 | 113084 | 100% | 1000000 |
| gemfibrozil | 0.22 ± 0.06 | 0.018 ± 0.006 | | 10 ± 1 | Razavi et al.[29] | 18 | 75 | 0.56% | 751000 |
| ketoprofen | 115 ± 60 | 0.21 ± 0.01 | 0.3 ± 0.01[28] | 3.5 ± 0.2 | Wols et al.[28] | 0.68 | 3.2 | 0.01% | 15600 |
| methylbenzotriazol | 0.09 ± 0.01 | 0.008 ± 0.002 | | 4.45 ± 1.11 | *this study* | 890.52 | 14175.66 | 27% | 75000 |
| metoprolol | 0.057 ± 0.005 | 0.071 ± 0.013 | 0.035 ± 0.04[28] | 7.5 | Wols et al.[28] | 1927 | 18595 | 70% | 3200 |
| metronidazol | 0.84 ± 0.05 | 0.003 ± 0.001 | 0.0034 ± 0.0001[28] | 4.7 ± 0.7 | Wols et al.[28] | 3.6 | 16 | 0.05% | 25000 |
| norfloxacin | 8.3 ± 2.1 | 0.032 ± 0.01 | 0.043 ± 0.005[30] | 1.7 ± 0.7 | *this study* | 0.33 | 1.5 | 0% | 40100 |
| ofloxacin | 1.1 ± 0.1 | 0.006 ± 0.001 | 0.0030 ± 0.0002[30] | 16 ± 4.7 | *this study* | 3.0 | 13 | 0.15% | 500 |
| paracetamol | 0.038 ± 0.004 | 0.010 ± 0.003 | 0.002 ± 0.003[28] | 7.1 ± 4.7 | Wols et al.[28] | 716 | 5698 | 22% | 9200 |
| primidon | n.a. | n.a. | | 6.7 ± 0.02 | Real et al.[31] | 4128 | 23947 | 100% | 54171 |
| propranolol | 0.60 ± 0.05 | 0.024 ± 0.005 | 0.0052[32] | 8.7 ± 0.3 | Chen et al.[33] | 12 | 91 | 0.43% | 50 |
| simvastatin | n.a. | n.a. | | 3.1 ± 0.2 | Razavi et al.[34] | 8810 | 51098 | 100% | 9600 |
| sotalol | 4.2 ± 0.3 | 0.39 ± 0.08 | | 1.6 ± 0.6 | *this study* | 0.98 | 4.1 | 0% | 15935 |
| sulfamethoxazol | 1.4 ± 0.1 | 0.028 ± 0.005 | 0.038 ± 0.011[28] | 5.1 ± 0.74 | Wols et al.[28] | 23 | 102 | 0.37% | 27 |
| trimethoprim | 0.46 ± 0.04 | 0.0007 ± 0.0002 | 0.001 ± 0.0001[28] | 6.3 ± 0.85 | Wols et al.[28] | 1545 | 16059 | 49% | 16000 |

## Modeling information

**Important model parameters (more details found in Razmi et al.[35])**

**Wind speed, direction:** Bise: 3 m $s^{-1}$, 10° ; Vent: 3 m $s^{-1}$, 240°
**Radius of release:** 10 m
**Vertical dispersion coefficient:** 0.0001-0.00001 (depending on the stratification)
**Density of water:** 1000 kg $m^3$
**Horizontal dispersion coefficient:** 0.3 $m^2$ $s^{-1}$ based on Peeters et al.[36]
**Stratification:** Thermocline around 14–16 m depth in Vidy Bay.

**Coupling photodegradation and hydrodynamics**

The spatial distribution of environmental concentrations near the outfall was estimated by combining particle tracking and photolysis kinetics. The modeled area of the Bay (4 km by 3 km, starting at the north-eastern coordinate 532,600/152,450, Swiss coordinate system) was discretized into a 50-by-50 m grid, over layers of 2 m depth. The hydrodynamic particle tracking model yielded the 3D position $p_{n,t,j}$ of each particle (parcel of water) $n$ (total of 5,000 particles released), for each time step $t$ (15 min intervals=$\Delta(t)$), up to 3 d following the time of release.

$$p_{n,t,j} = j^{th} \text{ component of the posititon for particle } n \text{ at time } t \tag{S12}$$

with $j = 1$: $x$-coordinate, $j = 2$: $y$-coordinate and $j = 3$: depth $z$ (in m)
The number of particles in each cell of the grid $(x, y, z)$ at each time step $t$ is then given by:

$$\mathrm{N}_{x,y,z,t} = \sum_n \delta_{p_{n,t,1},x}\, \delta_{p_{n,t,2},y}\, \delta_{p_{n,t,3},z} \qquad \begin{matrix} \text{with } x = 1,2,...,300 \\ y = 1,2,...,200 \\ z = 1,2,...,25 \end{matrix} \tag{S13}$$

$$\text{and with } \delta \text{ the Kronecker delta}: \delta_{\alpha,\beta} = \begin{cases} 1 & \text{if } \alpha = \beta, \\ 0 & \text{if } \alpha \neq \beta. \end{cases} \tag{S14}$$

Thereafter, the concentration of each substance in every cell of the grid was determined separately, for each timestep. To do so, all $n$ particles were attributed a hypothetical mass $\mathrm{M}_0^i$ at the time of release ($t = 0$). $\mathrm{M}_0^i$ is compound-dependent, and chosen such that the sum of all particle masses in the release volume match the concentration of a given compound ($i$) that was actually observed during the 2010 sampling campaign (i.e. the concentrations measured in the surface plume in November 2010 were used for the unstratified scenario and those detected in June 2010 for the stratified scenario).

Assuming no degradation, the mass of each particle is constant in time, and the concentration of compound $i$ in a given cell $(x, y, z)$ at a specific timepoint $t$ is given by:

$$\mathrm{C}^{conservative,i}_{x,y,z,t} = \frac{\mathrm{N}_{x,y,z,t}\,\mathrm{M}^{i}_{0}}{\mathrm{V}} \tag{S15}$$

where V is the cell volume (50 × 50 × 2 m). In this conservative case, only dilution affects the concentration in each cell of the modelled area.
However, most compounds being susceptible to photodegradation, each of the 5,000 particles released undergoes a depth-dependent degradation. Hence, the mass of each particle evolves over time according to its relative distance from the surface, following a first-order degradation:

$$\mathrm{M}^{i}_{n,t} = \mathrm{M}^{i}_{0}\, e^{-\Delta t \cdot \sum_{\tilde{t}=0}^{t-1} k^{i}_{n,\tilde{t}}} \tag{S16}$$

with $\Delta t$ = 15 min, and $k^{i}_{n,\tilde{t}}$ the depth-dependent degradation rate constant of particle $n$ for a given micropollutant $i$. $k^{i}_{n,\tilde{t}}$ was calulated according to equation 5 (in text) and is a function of the propensity of compound $i$ to undergo photolysis, the incoming irradiance, $\mathrm{I}_{sun}$ (summer or winter), and the depth. Due to the finite resolution, we used the average depth between timesteps $(p_{n,\tilde{t},3} + p_{n,\tilde{t}-1,3}/2)$:

$$k^{i}_{n,\tilde{t}} = f(i, p_{n,\tilde{t},3}, p_{n,\tilde{t}-1,3}, \mathrm{I}_{sun}) \tag{S17}$$

When both dilution and photolysis processes are considered, the concentration of compound $i$ in a given cell at time $t$ is:

$$\mathrm{C}^{photo,i}_{x,y,z,t} = \frac{\sum_{n} \delta_{p_{n,t,1},x}\, \delta_{p_{n,t,2},y}\, \delta_{p_{n,t,3},z}\, \mathrm{M}^{i}_{n,t}}{\mathrm{V}} \tag{S18}$$

Finally, to reflect the actual conditions of effluent WW discharge in Vidy Bay, which is continuous and not instantaneous, a continuous release situation was mimicked by addition of the concentrations in each cell over all timesteps, until reaching steady state conditions. Accordingly the steady state predicted environmental concentration (PEC) in a given cell assuming only dilution processes (cloudy skies) is given by:

$$\mathrm{PEC}^{conservative,i,ss}_{x,y,z} = \sum_{t} \mathrm{C}^{conservative,i}_{x,y,z,t} \tag{S19}$$

When both dilution and photodegradation are occurring, the predicted environmental concentration becomes:

$$\mathrm{PEC}^{photo,i,ss}_{x,y,z} = \sum_{t} \mathrm{C}^{photo,i}_{x,y,z,t} \tag{S20}$$

# Additional modeling results

## Time to steady state

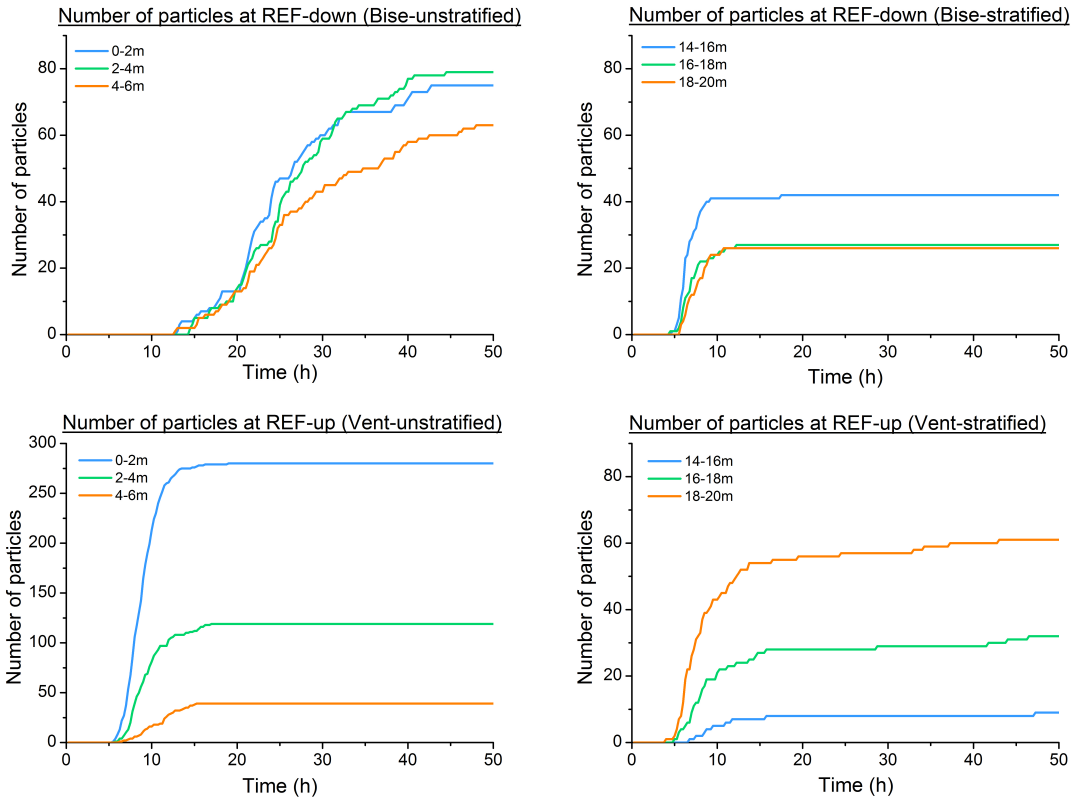


Figure S. 8: *Number of particles over time in different layers at REF-down (top figures) and REF-up (bottom figures) for the Bise and Vent scenarios, respectively. The initial increase of particles indicates the minimal travel-time from the WWTP outfall to the considered reference location. Steady state is reached once the number of particle stabilizes.*

## Concentration-depth profiles for Vent conditions

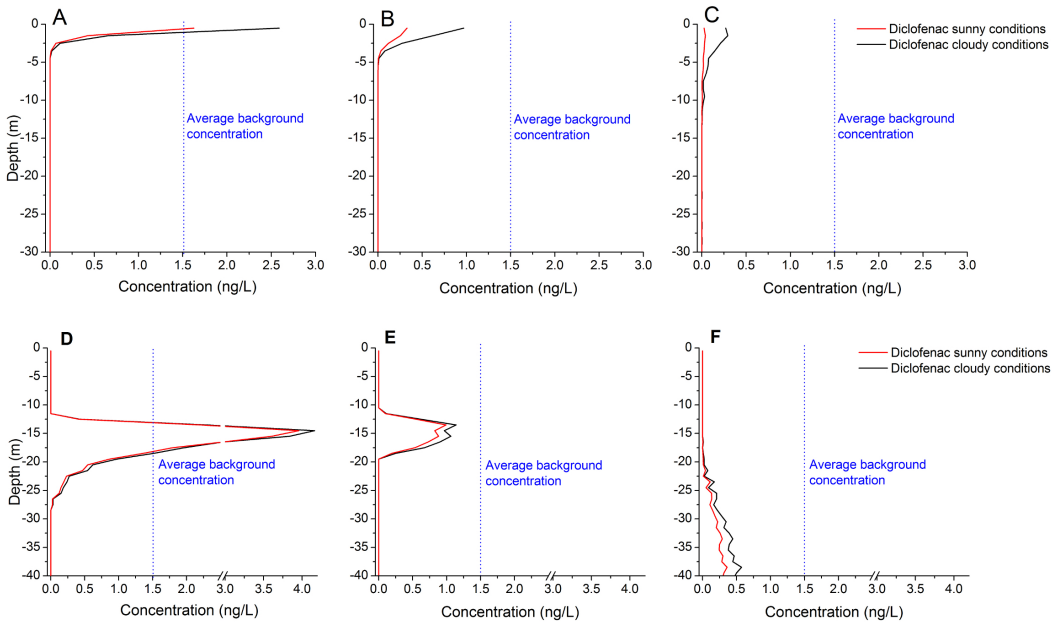


Figure S. 9: *Modeled concentration-depth profiles for diclofenac under unstratified Vent (top), and stratified Vent (bottom) for the locations A-F marked by blue crosses in Figure 2.*

## Concentration depth profiles for Bise conditions

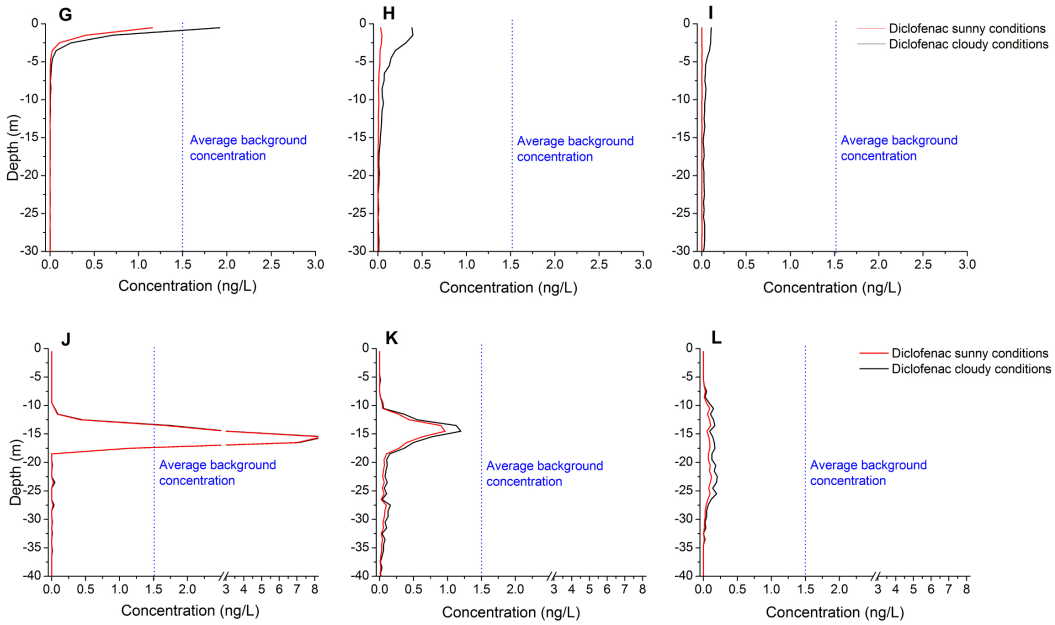


Figure S. 10: *Modeled concentration-depth profiles for diclofenac under unstratified Bise (top), and stratified Bise (bottom) for the locations G-L marked by blue crosses in Figure 2.*

**Spatial extent of the diclofenac concentration exceeding the background concentration**

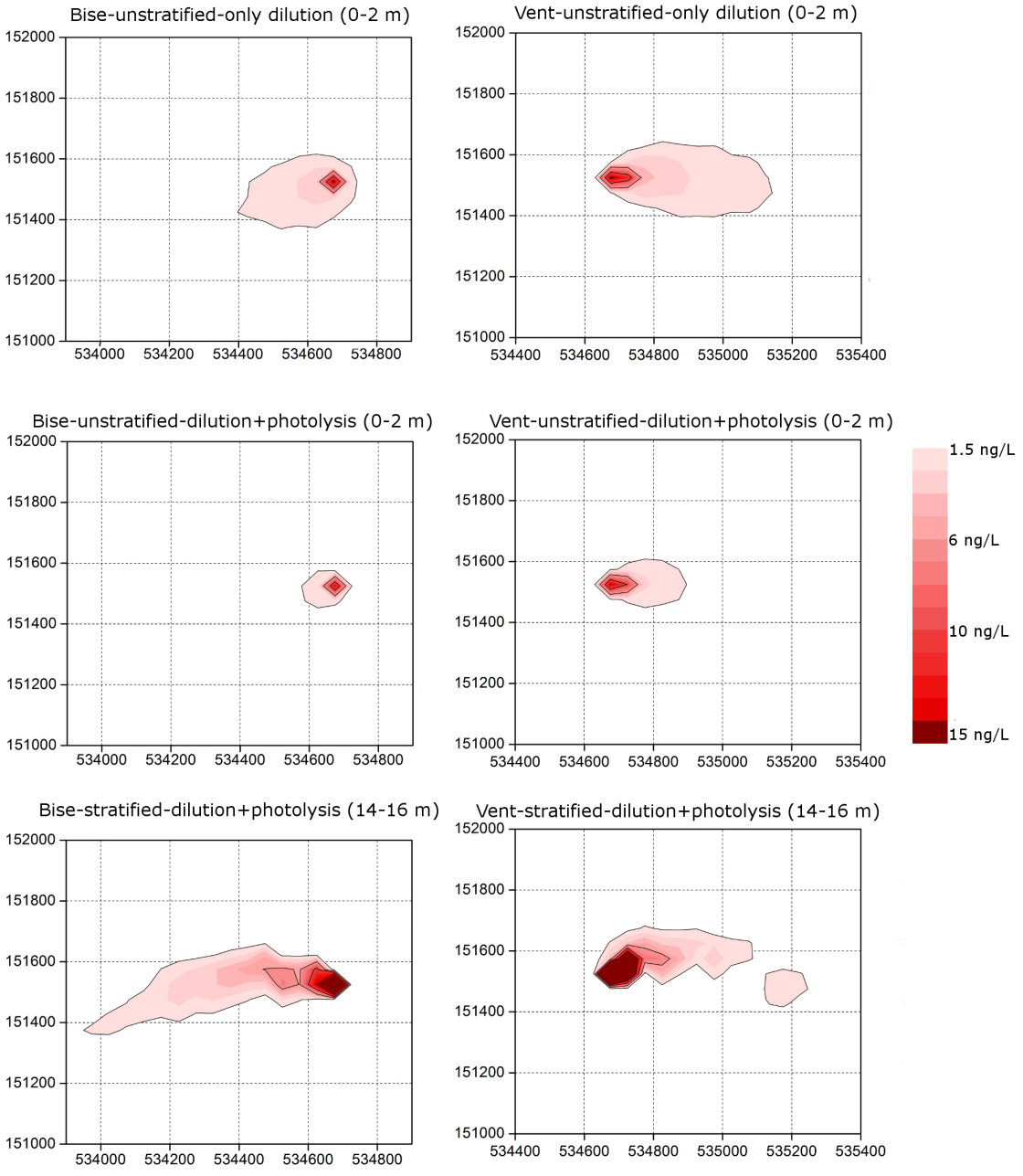


Figure S. 11: *Spatial extent of the diclofenac concentration which exceeds the lake background concentration (1.5 ng $L^{-1}$) for the different wind conditions: Bise (left panel) and Vent (right panel); and climatic scenarios: well-mixed cloudy conditions (top), well-mixed sunny conditions (middle) and stratified sunny conditions (bottom). Axes show the latitudinal and longitudinal coordinates (Swiss Grid system with datum CH1903)*

**3D extension of the risk quotient for the stratified Vent scenario**

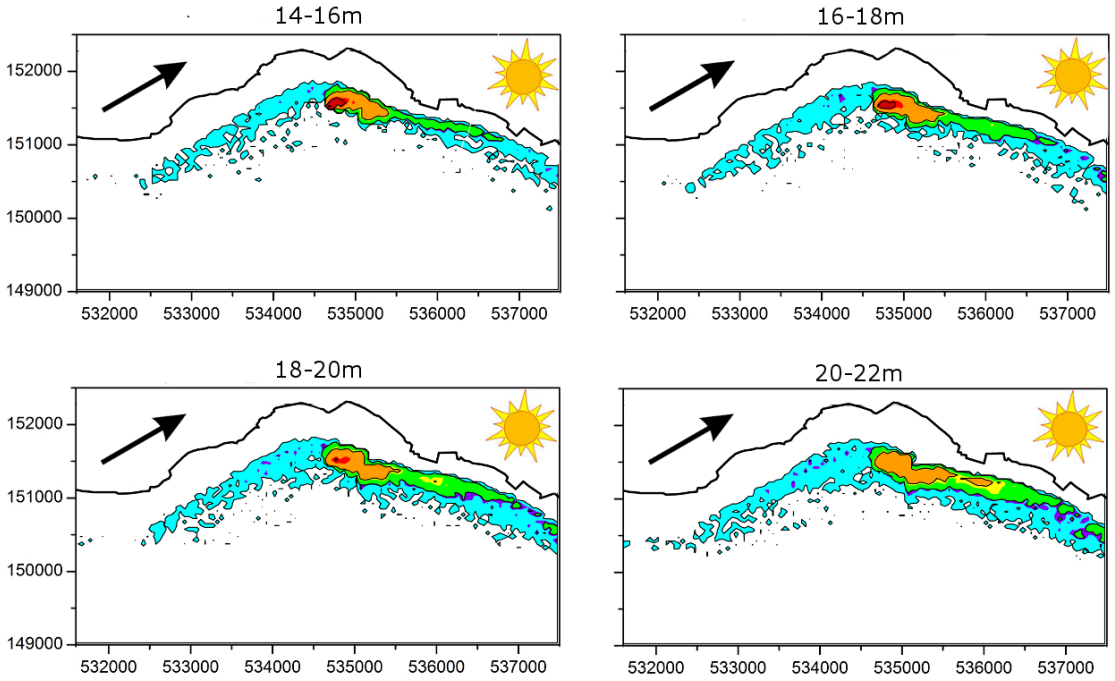


Figure S. 12: *3D extension of the risk quotient for the stratified Vent scenario. The highest risk (red) is observed in the release layer (14–16 m), but the precautionary risk zone (orange) extends further at lower depths (20–22 m). Arrows indicate the wind direction and axes show the latitudinal and longitudinal coordinates (Swiss Grid system with datum CH1903).*

## References


1. PhysPropDatabase, http://www.syrres.com/what-we-do/databaseforms.aspx?id=386.
2. ToxicologyDataNetwork, http://toxnet.nlm.nih.gov/index.html.
3. Meylan, W.; Howard, P. *Environ. Toxicol. Chem.* **1991**, *10*, 1283–1293.
4. Liu, Y.; Ying, G.; Shareef, A.; Kookana, R. *Water Res.* **2011**, *45*, 5005–5014.
5. Chemicalland21, http://www.chemicalland21.com/.
6. Kummerer, K. *J. Environ. Manage.* **2009**, *90*, 2354–2366.
7. Hoppe-Jones, C.; Dickenson, E. R.; Drewes, J. E. *Sci. Total Environ.* **2012**, *437*, 137 – 144.
8. Bonvin, F.; Rutler, R.; Chevre, N.; Halder, J.; Kohn, T. *Environ. Sci. Technol.* **2011**, *45*, 4702–4709.
9. Fono, L. J.; Kolodziej, E. P.; Sedlak, D. L. *Environ. Sci. Technol.* **2006**, *40, 23*, 7257–7262.
10. Haggard, B. E.; Bartsch, L. D. *J. Environ. Quality* **2009**, *38*, 343–352.
11. Radke, M.; Ulrich, H.; Wurm, C.; Kunkel, U. *Environ. Sci. Technol.* **2010**, *44*, 2968–2974.
12. Kunkel, U.; Radke, M. *Water Res.* **2012**, *46*, 5551–5565.
13. Kunkel, U.; Radke, M. *Environ. Sci. Technol.* **2011**, *45, 15*, 6296–6302.
14. Razmi, A. M.; Barry, D. A.; Bakhtyar, R.; Le Dantec, N.; Dastgheib, A.; Lemmin, U.; Wuest, A. *J. Great Lakes Res.* **2013 (in press)**,
15. Haldiman, S. Modelisation des rejoets hydrauliques pollutifs sur le littoral Lausannois. M.Sc. thesis, EPFL, 2009.
16. Meteosuisse, www.meteosuisse.admin.ch, last accessed 26 February 2013.
17. Morasch, B.; Bonvin, F.; Reiser, H.; Grandjean, D.; de Alencastro, L. F.; Perazzolo, C.; Chevre, N.; Kohn, T. *Environ. Toxicol. Chem.* **2010**, *29*, 1658–1668.
18. Leifer, A. *The Kinetics of Environmental Aquatic Photochemistry : Theory and Practice*; American Chemical Society: Washington, DC, 1988.
19. Schwarzenbach, R. P.; Gschwend, P. M.; Imboden, D. M. *Environmental Organic Chemistry, 2nd Edition.*; John Wiley &L Sons, Inc., 2003.
20. Brezonik, P. L.; Fulkerson-Brekken, J. *Environ. Sci. Technol.* **1998**, *32*, 3004–3010.
21. Lazzarotto, J.; Nirel, P.; Rapin, F. *Physical-chemical changes in the waters of Lake Geneva (major elements). Campagne 2010.*; 2011.
22. Larson, R. A.; Zepp, R. G. *Environ. Toxicol. Chem.* **1988**, *7*, 265–274.

23. Ji, Y.; Zeng, C.; Ferronato, C.; Chovelon, J.-M.; Yang, X. *Chemosphere* **2012**, *88*, 644–649.

24. Dodd, M. C.; Kohler, H.-P. E.; Von Gunten, U. *Environ. Sci. Technol.* **2009**, *43*, 2498–2504.

25. Andreozzi, R.; Caprio, V.; Insola, A.; Longo, G. *J. Chem. Technol. Biotech.* **1998**, *73*, 93–98.

26. Vel Leitner, N. K.; Roshani, B. *Water Res.* **2010**, *44*, 2058–2066.

27. Huber, M. M.; Canonica, S.; Park, G. Y.; Von Gunten, U. *Environ. Sci. Technol.* **2003**, *37*, 1016–1024.

28. Wols, B. A.; Hofman-Caris, C. H. M. *Water Res.* **2012**, *46*, 2815–2827.

29. Razavi, B.; Song, W.; Cooper, W. J.; Greaves, J.; Jeong, J. *J. Phys. Chem. A* **2009**, *113*, 1287–1294.

30. Wammer, K. H.; Korte, A. R.; Lundeen, R. A.; Sundberg, J. E.; McNeill, K.; Arnold, W. A. *Water Res.* **2013**, *47*, 439–48.

31. Real, F. J.; Benitez, F. J.; Acero, J. L.; Sagasti, J. J. P.; Casas, F. *Ind. Eng. Chem. Res.* **2009**, *48*, 3380–3388.

32. Lin, A. Y. C.; Reinhard, M. *Environ. Toxicol. Chem.* **2005**, *24*, 1303–1309.

33. Chen, Y.; Hu, C.; Hu, X.; Qu, J. *Environ. Sci. Technol.* **2009**, *43*, 2760–2765.

34. Razavi, B.; Ben Abdelmelek, S.; Song, W.; O'Shea, K. E.; Cooper, W. J. *Water Res.* **2011**, *45*, 625–631.

35. Razmi, A. M.; Barry, D. A.; Lemmin, U.; Bonvin, F.; Kohn, T.; Bakhtyar, R. *Aquatic Sci.* **2013 (in revision)**,

36. Peeters, F.; Wuest, A.; Piepke, G.; Imboden, D. *J. Geophys. Res. Oceans* **1996**, *101*, 18361–18375.